Adaptive three-step Kalman filter for air data sensor fault detection and diagnosis

Lu, P; van Eykeren, L; van Kampen, EJ; de Visser, CC; Chu, QP

DOI
10.2514/1.G001313

Publication date
2016

Document Version
Accepted author manuscript

Published in
Journal of Guidance, Control, and Dynamics: devoted to the technology of dynamics and control

Adaptive Three-Step Kalman Filter for Air Data Sensor Fault Detection and Diagnosis

P. Lu[1], L. Van Eykeren[2], E. van Kampen[3], C.C. de Visser[4], Q.P. Chu[5]
Delft University of Technology, P.O. Box 5058, 2600 GB Delft, The Netherlands

Air Data Sensor (ADS) Fault Detection and Diagnosis (FDD) is important for the safety of aircraft. In this paper, first an extension of the Robust Three-Step Kalman Filter (RTS-KF) to nonlinear systems is made by proposing a Robust Three-Step Unscented Kalman Filter (RTS-UKF). The RTS-UKF is found to be sensitive to the initial condition error when dealing with ADS fault estimation. A theoretical analysis of this sensitivity is presented and a novel Adaptive Three-Step Unscented Kalman Filter (ATS-UKF) is proposed which is able to cope with not only the estimation of the ADS faults but also the detection and isolation of faults. The ATS-UKF contains three steps: time update, fault estimation and measurement update. This approach can reduce the sensitivity to the initial condition error. Finally, the ADS FDD performance of the ATS-UKF is validated using simulated aircraft data. Additionally, its performance is further validated using real flight test data to demonstrate its performance under realistic uncertainties and disturbances. The results using both the simulated data and real flight test data demonstrate the satisfactory FDD performance of the ATS-UKF and verify that it can be applied in practice to enhance the safety of aircraft.

---

[1] Ph.D. Student, Control and Simulation Division; P.Lu-1@tudelft.nl.
[2] Ph.D. Student, Control and Simulation Division; L.VanEykeren@tudelft.nl
[3] Assistant Professor, Control and Simulation Division; e.vankampen@tudelft.nl
[4] Assistant Professor, Control and Simulation Division; c.c.devisser@tudelft.nl
[5] Associate Professor, Control and Simulation Division; q.p.chu@tudelft.nl

Nomenclature

A_x, A_y, A_z = linear accelerations along the body axis, m/s^2

A_{xm}, A_{ym}, A_{zm} = measurements of linear accelerations along the body axis, m/s^2

T = thresholds for detecting faults

V = true airspeed, m/s

V_m, α_m, β_m = air data sensor measurements

f = output faults

$\hat{f}$ = estimation of output faults

f_V, f_α, f_β = faults in the air data sensors

p, q, r = roll, pitch and yaw rate along the body axis, rad/s

p_m, q_m, r_m = measurements of roll, pitch and yaw rate along the body axis, rad/s

α, β = angle of attack, sideslip angle, rad

α_{vm}, β_{vm} = angle of attack, sideslip angle measurements from the vane, rad

γ = innovation of the filter

ϕ, θ, ψ = roll, pitch and yaw angles along the body axis, rad

ϕ_m, θ_m, ψ_m = measurements of roll, pitch and yaw angles along the body axis, rad

L, l, m, p = dimensions of the state, input, output and output faults, respectively

$\hat{x}$, P = state estimate and its error covariance matrix of the filter

I. Introduction

PRESENTLY, Fault Detection and Isolation (FDI) has an important role in achieving fault-tolerance of aircraft [1]. During the past few decades, many approaches have been proposed for sensor or actuator FDI [2–4]. In aerospace engineering, the FDI of sensors and actuators for fixed-wing aircraft is widely studied, as can be found in Patton [1], Marzat et. al [5], and Hajiyev and Caliskan [6]. Investigation of the FDI for Unmanned Aerial Vehicles can also be found [5, 7]. For recent advances, the reader is referred to Goupil [8] and Zolghadri [9, 10]. The Air Data Sensors (ADSs) measure the dynamic pressure, airspeed, angle of attack and angle of sideslip of the aircraft, providing essential information on the aircraft states to the pilot [11]. The ADSs are usually

installed outside the aircraft fuselage and can suffer from icing or water accumulation, which may result in faults such as blockage faults [12]. These faults may negatively influence the information provided to the pilot, which can lead to catastrophic accidents. In the recent past, there have been commercial aircraft accidents caused by ADS faults. Due to faults in the ADSs, the flight crew of Austral Lineas Aeroeas Flight 2553 improperly referenced the airspeed indicator and induced a structure failure by exceeding safe airspeed limits [13]. More recently, the final report of the Air France Flight 447 accident stated that erroneous airspeed measurements from the pitot probes were a contributing factor [14]. Since 2003, commercial aircraft have had more than 35 recorded incidents of multiple ADS faults [13]. There have also been accidents of military aircraft caused by ADS faults. The crash of a B-2 bomber is due to a large bias to the ADSs which is caused by moisture in the port transducer units [14]. These facts indicates the importance of the fault detection of the ADSs.

The fault detection of ADSs has been investigated in a number of studies [12, 15]. Some researchers propose to use alternative air data sensing systems such as a flush air-data sensing system [15, 16]. Nebula et. al propose a virtual air data system against ADS failures [17, 18]. Looye and Joos [19] propose to use the data from a navigation system to determine the air data information. On the other hand, the faults of the ADSs can be detected. Houck and Atlas [11] are one of the first to analyze ADS faults. The limitation of their approach is that independent static pressure measurements are not always available in Unmanned Aerial Vehicle (UAV) applications [13]. Cervia et al. [20] and Eubank et al. [13] detect the faults using a multiple-redundancy air data system. The air data system studied by Cervia et al. is based on pseudo-quadruplex redundancy which employs four self-aligning air data probes. Freeman et al. [12] investigate analytical redundancy instead of hardware redundancy for the ADS fault detection. They use a longitudinal dynamics model of the aircraft and two linear H_∞ filters are designed to detect the faults and provide robustness to model errors.

Alternatively, the kinematic model can be used to detect the faults in the ADSs, thereby reducing the influence of model uncertainties caused by the calculation of the aerodynamic forces and moments [21, 22]. Van Eykeren and Chu [23] use an adaptive Extended Kalman Filter to detect the faults

in the ADSs. However, the estimation of the faults is not addressed in their work. In Lu et al. [24], a Selective-Reinitialization Multiple-Model Adaptive Estimation approach is proposed for the ADS Fault Detection and Diagnosis (FDD). The approach improved the FDD performance of the Multiple-Model-based approaches. However, the computational load of the approach is intensive when dealing with simultaneous faults.

In this paper, a newly-developed Robust Three-Step Kalman Filter (RTS-KF) [25] is combined with the kinematic model to estimate the ADS faults. First, the RTS-KF is extended to cope with nonlinear systems by proposing a novel Robust Three-Step Unscented Kalman Filter (RTS-UKF). The RTS-UKF is able to reduce linearization error. However, it is found that the RTS-UKF is sensitive to the initial condition errors. Second, the sensitivity of this three-step Kalman Filter to the initial condition error is analyzed theoretically. It is proved that the RTS-UKF does not use some of the measurements to update the state estimation which causes the sensitivity to the initial condition error.

Finally, a novel Adaptive Three-Step Unscented Kalman Filter (ATS-UKF) is proposed which does not only estimate the ADS faults, but also detect and isolate the faults. The ATS-UKF contains three steps: time update, fault estimation and measurement update. The fault detection is performed before the fault estimation. This approach also reduces its sensitivity to the initial condition. The fault detection is performed by checking the innovation variances. In the presence of faults, the innovation variance increases. If the innovation variance exceeds a pre-defined threshold, then the fault alarm is triggered. The FDD performance of the ATS-UKF is tested using simulated aircraft data with the objective of detecting, isolating and estimating ADS faults. Two different fault scenarios (multiple faults and simultaneous faults) are implemented to test the performance and the results demonstrate the satisfactory performance of the ATS-UKF. The fault types contain not only bias and drift fault, but also oscillatory faults.

Furthermore, the FDD performance of the ATS-UKF is validated using real flight test data of a Cessna Citation II aircraft. The sensor measurements from the real flight test contain biases and uncertainties and are suitable for testing the performance of the ATS-UKF. Different fault scenarios are generated and the faults are injected into the real flight data. The ADS FDD results of the

ATS-UKF demonstrate its performance and verified that it can be applied in practice to enhance the safety of the aircraft.

The structure of the paper is as follows: In Section II, the ADS FDD problem is formulated. The kinematic model including ADS faults is introduced. Section III extends the RTS-KF to cope with nonlinear systems by proposing the RTS-UKF. The RTS-UKF is applied to estimate the ADS faults, which turns out to be sensitive to the initial condition. The sensitivity problem is analyzed theoretically and a novel ATS-UKF is proposed to deal with not only the estimation of the ADS faults, but also the detection and isolation of the faults. The performance is tested using a simulated aircraft model. In Section IV, the performance of the ATS-UKF is further validated using the real flight data of the Cessna Citation II aircraft. The performance is shown and some remarks are given. Finally, the conclusions are made in Section V.

II. Air Data Sensor FDD using the kinematic model

The objective of this paper is the FDD of the aircraft ADSs. However, model-based approaches are sensitive to model uncertainties. In order to make the proposed approach more robust, the kinematic model of aircraft, which does not involve the computation of aerodynamic forces and moments, is used instead of the aerodynamic model.

A. Aircraft kinematic model with ADS faults

The kinematic model of the aircraft including ADS faults is described as

$$\dot{x}(t) = \bar{f}(x(t), u_m(t), t) + G(x(t))w(t) \tag{1}$$

$$y(t) = h(x(t), u_m(t), t) + v(t) + F(t)f(t) \quad t = t_i, \ i = 1, 2, ... \tag{2}$$

where $x \in \mathbb{R}^L$ represents the system states, $u_m \in \mathbb{R}^l$ the measured input, $y \in \mathbb{R}^m$ the measurement. The functions $\bar{f}$ and h are nonlinear functions. G and F are the noise distribution matrix and output fault distribution matrix. The function $f \in \mathbb{R}^p$ represents output faults.

The system equation variables are defined as follows:

$$x = [V\ \alpha\ \beta\ \phi\ \theta\ \psi]^T \tag{3}$$

$$u_m = [A_{xm}\ A_{ym}\ A_{zm}\ p_m\ q_m\ r_m\ ]^T = [A_x\ A_y\ A_z\ p\ q\ r\ ]^T + w \tag{4}$$

$$y = [V_m\ \alpha_m\ \beta_m\ \phi_m\ \theta_m\ \psi_m]^T \tag{5}$$

$$w = [w_x\ w_y\ w_z\ w_p\ w_q\ w_r\ ]^T \tag{6}$$

$$v = [v_V\ v_\alpha\ v_\beta\ v_\phi\ v_\theta\ v_\psi]^T \tag{7}$$

$$f = [f_V\ f_\alpha\ f_\beta]^T \tag{8}$$

where the input u_m is the Inertial Measurement Unit (IMU) measurement which measures the linear accelerations (A_x, A_y and A_z) and angular rates (roll rate p, pitch rate q, and yaw rate r) of the aircraft. y is the output measurement which measures the air data information (true airspeed V, angle of attack α, and angle of sideslip β) and Euler angles (roll angle ϕ, pitch angle θ, and yaw angle ψ). $[f_V\ f_\alpha\ f_\beta]^T$ are the faults of the ADSs, i.e. f_V, f_α and f_β are the faults in the velocity sensor, angle of attack sensor, and angle of sideslip sensor, respectively. It is assumed that there are no faults in the Attitude and Heading Reference System which measures the Euler angles and the influence of changing wind such as turbulence is limited. Therefore, the input noise vector $w(t)$ can be assumed to be a continuous time white noise process while the output noise vector $v(t)$ can be assumed to be a discrete time noise sequence.

$$E[w(t)] = 0$$

$$E[w(t)w^T(t_\tau)] = Q\delta(t-\tau)\ ,\ Q = \mathrm{diag}(\sigma^2_{w_x},\ \sigma^2_{w_y},\ \sigma^2_{w_z},\ \sigma^2_{w_p},\ \sigma^2_{w_q},\ \sigma^2_{w_r}), \tag{9}$$

$$E[v(t)] = 0$$

$$E[v(t_i)v^T(t_j)] = R\delta(t_i-t_j)\ ,\ R = \mathrm{diag}(\sigma^2_{v_V},\ \sigma^2_{v_\alpha},\ \sigma^2_{v_\beta},\ \sigma^2_{v_\phi},\ \sigma^2_{v_\theta},\ \sigma^2_{v_\psi}), \tag{10}$$

$$E[w(t)v^T(t_i)] = 0\ ,\ t = t_i\ ,\ i = 1, 2, ... \tag{11}$$

The kinematic model is given as follows [23, 24]:

$$\dot{V} = (A_{xm} - w_{Ax} - g\sin\theta)\cos\alpha\cos\beta + (A_{ym} - w_{Ay} + g\sin\phi\cos\theta)\sin\beta + (A_{zm} - w_{Az} + g\cos\phi\cos\theta)\sin\alpha\cos\beta \tag{12}$$

$$\dot{\alpha} = \frac{1}{V\cos\beta}\big[-(A_{xm} - w_{Ax})\sin\alpha + (A_{zm} - w_{Az})\cos\alpha + g\cos\phi\cos\theta\cos\alpha + g\sin\theta\sin\alpha\big] + q_m - w_q - [(p_m - w_p)\cos\alpha + (r_m - w_r)\sin\alpha]\tan\beta \tag{13}$$

$$\dot{\beta} = \frac{1}{V}\big[-(A_{xm} - w_{Ax} - g\sin\theta)\cos\alpha\sin\beta + (A_{ym} - w_{Ay} + g\sin\phi\cos\theta)\cos\beta - (A_{zm} - w_{Az} + g\cos\phi\cos\theta)\sin\alpha\sin\beta\big] + (p_m - w_p)\sin\alpha - (r_m - w_r)\cos\alpha \tag{14}$$

$$\dot{\phi} = (p_m - w_p) + (q_m - w_q)\sin\phi\tan\theta + (r_m - w_r)\cos\phi\tan\theta \tag{15}$$

$$\dot{\theta} = (q_m - w_q)\cos\phi - (r_m - w_r)\sin\phi \tag{16}$$

$$\dot{\psi} = (q_m - w_q)\frac{\sin\phi}{\cos\theta} + (r_m - w_r)\frac{\cos\phi}{\cos\theta} \tag{17}$$

and $G(x(t))$ is defined as:

$$G(x(t)) = \begin{bmatrix} -\cos\alpha\cos\beta & -\sin\alpha\cos\beta & -\sin\alpha\cos\beta & 0 & 0 & 0 \\ \sin\alpha/(V\cos\beta) & 0 & -\cos\alpha/(V\cos\beta) & \cos\alpha\tan\beta & -1 & \sin\alpha\tan\beta \\ \cos\alpha\sin\beta/V & -\cos\beta/V & \sin\alpha\sin\beta/V & -\sin\alpha & 0 & \cos\alpha \\ 0 & 0 & 0 & -1 & -\sin\phi\tan\theta & -\cos\phi\tan\theta \\ 0 & 0 & 0 & 0 & -\cos\phi & \sin\phi \\ 0 & 0 & 0 & 0 & -\sin\phi/\cos\theta & -\cos\phi/\cos\theta \end{bmatrix} \tag{18}$$

Therefore, the measurement model including the ADS faults is

$$V_m = V + f_V + v_V \tag{19}$$

$$\alpha_m = \alpha + f_\alpha + v_\alpha \tag{20}$$

$$\beta_m = \beta + f_\beta + v_\beta \tag{21}$$

$$\phi_m = \phi + v_\phi \tag{22}$$

$$\theta_m = \theta + v_\theta \tag{23}$$

$$\psi_m = \psi + v_\psi \tag{24}$$

Table 1: Fault scenario of multiple faults

Time interval	Sensor	Fault type	Fault magnitude	Fault unit
10 s $< t <$ 20 s	V	bias	2	[m/s]
30 s $< t <$ 40 s	α	drift	$0.01t$	[rad/s]
50 s $< t <$ 60 s	β	oscillatory	$-2\pi \sin(\pi t)/180$	[rad]

The measurement model can be rewritten into

$$y(t) = x(t) + F(t)f(t) + v(t), \qquad t = t_i, i = 1, 2, ... \tag{25}$$

where

$$F = [I_3 \ 0_{3\times 3}]^T \tag{26}$$

The objective of the ADS FDD problem is to detect, isolate and estimate $f = [f_V \ f_\alpha \ f_\beta]^T$. This paper assumes that there are no faults in the IMU sensors. If there are faults in the IMU sensors, they can be detected and estimated by other methods using another set of kinematic model [26].

B. Fault scenarios for the ADS FDD

In this paper, two different fault scenarios are used to test the performance of the approaches. The fault scenario for multiple ADS faults is given in Table 1 while that for simultaneous ADS faults is given in Table 2. The fault type, magnitude and unit are given in the table. The units of the drift faults are given by the units of the drift rates. It can be seen that the fault types not only contains bias faults but also drift faults and oscillatory faults.

C. State observability and fault reconstructibility

This section check the observability of the system described by Eqs. (1) and (2). The observability analysis of the system can be performed by checking the rank of the following observability

Table 2: Fault scenario of simultaneous faults

Time interval	Sensor	Fault type	Fault magnitude	Fault unit
	V	oscillatory	$2\sin(\pi t)$	[m/s]
$10\text{ s} < t < 20\text{ s}$	α	drift	$0.01t$	[rad/s]
	β	drift	$-0.01t$	[rad/s]
	V	drift	$-0.2t$	[m/s^2]
$30\text{ s} < t < 40\text{ s}$	α	bias	$-2\pi/180$	[rad]
	β	oscillatory	$-2\pi\sin(\pi t)/180$	[rad]

matrix:

$$O = \begin{bmatrix} \delta_x h \\ \delta_x(L_{\bar{f}}h) \\ \vdots \\ \delta_x(L_{\bar{f}}^{L-1}h) \end{bmatrix} \tag{27}$$

where the Lie derivative is defined as follows:

$$\begin{aligned} L_{\bar{f}}h &= \delta_x h \cdot \bar{f} \\ &\vdots \\ L_{\bar{f}}^{L-1}h &= \delta_x(L_{\bar{f}}^{L-2}h) \cdot \bar{f} \end{aligned} \tag{28}$$

It can be readily checked that O is of full rank. Therefore, the system state is observable. In order to reconstruct the faults, additional conditions are required which are given in (29).

III. Extension of the Robust Three-Step Kalman Filter

This section extends the RTS-KF to estimate output faults. First, in Section III A, the RTS-KF is extended to nonlinear systems by proposing a RTS-UKF. This RTS-UKF is applied to the ADS fault estimation problem and is found to be sensitive to the initial condition errors. This sensitivity problem is analyzed theoretically in Section III B. Then, in Section III C, an ATS-UKF is proposed which can detect, isolate and estimate the faults. Finally, the ATS-UKF is applied to the ADS FDD problem in Section III D to demonstrate its FDD performance.

A. Robust Three-Step Unscented Kalman Filter

The RTS-KF [25] can be used for output FDD. Consider the aircraft kinematic model described by Eqs. (1) and (2). For this system, since the system state is observable, the existence condition of a RTS-KF is [25]:

$$m \geq p, \qquad \text{rank } F_k = p \tag{29}$$

In this study, $m = 6$, $p = 3$ and rank $F_k = 3$. Therefore, a RTS-KF can be designed to estimate the ADS faults.

However, the RTS-KF is designed for linear systems while the kinematic model is nonlinear. Therefore, the RTS-KF needs to be extended to cope with nonlinear systems. The Unscented Kalman Filter (UKF) is a nonlinear filter which can achieve a better level of accuracy than the Extended Kalman Filter (EKF) [27, 28]. This section extends the RTS-KF to nonlinear systems by proposing a RTS-UKF.

According to the technique in Lu et al. [22], the RTS-UKF can be derived as follows:

Step1 Sigma points calculation and time update

$$\mathcal{X}_{0,k-1} = \hat{x}_{k-1|k-1} \tag{30a}$$

$$\mathcal{X}_{i,k-1} = \hat{x}_{k-1|k-1} - (\sqrt{(L+\gamma_0)P_{k-1|k-1}})_i, \quad i = 1, 2, ..., L \tag{30b}$$

$$\mathcal{X}_{i,k-1} = \hat{x}_{k-1|k-1} + (\sqrt{(L+\gamma_0)P_{k-1|k-1}})_i, \quad i = L+1, L+2, ..., 2L \tag{30c}$$

$$w_0^{(m)} = \gamma_0/(L+\gamma_0) \tag{31a}$$

$$w_0^{(c)} = \gamma_0/(L+\gamma_0) + (1 - \alpha_0^2 + \beta_0) \tag{31b}$$

$$w_i^{(m)} = w_i^{(c)} = 1/\{2(L+\gamma_0)\}, \quad i = 1, 2, ..., 2L \tag{31c}$$

with $\mathcal{X}_{i,k-1}$ the sigma points of the states (dimension L) at step $k-1$. $w_i^{(m)}$ and $w_i^{(c)}$ are the weights associated with the ith point with respect to $\hat{x}_{k-1|k-1}$ and $P_{k-1|k-1}$, respectively. $\gamma_0 = \alpha_0^2(L+\kappa) - L$ is a scaling factor, α_0 determines the spread of the sigma points around $\hat{x}_{k-1|k-1}$, κ is a secondary scaling factor, β_0 is used to incorporate the prior knowledge of the distribution of x. In this paper, $\kappa = 0$, $\alpha_0 = 0.8$ and $\beta_0 = 2$.

After the creation of the sigma points through the nonlinear transformation, the predicted mean and covariance are computed as follows

$$\mathcal{X}_{i,k|k-1} = \mathcal{X}_{i,k-1} + \int_{k-1}^{k} \bar{f}(\mathcal{X}_{i,k-1}, u(t), t)dt \tag{32}$$

$$\hat{x}_{k|k-1} = \sum_{i=0}^{2L} w_i^{(m)} \mathcal{X}_{i,k,k-1} \tag{33}$$

$$P_{k|k-1} = \sum_{i=0}^{2L} w_i^{(c)} [\mathcal{X}_{i,k|k-1} - \hat{x}_{k|k-1}][\mathcal{X}_{i,k|k-1} - \hat{x}_{k|k-1}]^T + Q \tag{34}$$

$$\mathcal{X}^*_{i,k|k-1} = [\mathcal{X}_{0:2L,k|k-1} \quad \mathcal{X}_{0,k|k-1} - \nu\sqrt{Q} \quad \mathcal{X}_{0,k|k-1} + \nu\sqrt{Q}]_i \tag{35}$$

$$\mathcal{Y}^*_{i,k|k-1} = h(\mathcal{X}^*_{i,k|k-1}) \tag{36}$$

$$\hat{y}_k = \sum_{i=0}^{2L^a} w_i^{*(m)} \mathcal{Y}^*_{i,k|k-1} \tag{37}$$

$$P_{xy,k} = \sum_{i=0}^{2L^a} w_i^{*(c)} [\mathcal{X}_{i,k|k-1} - \hat{x}_{k|k-1}][\mathcal{Y}_{i,k|k-1} - \hat{y}_k]^T \tag{38}$$

$$P_{yy,k} = \sum_{i=0}^{2L^a} w_i^{*(c)} [\mathcal{Y}_{i,k|k-1} - \hat{y}_k][\mathcal{Y}_{i,k|k-1} - \hat{y}_k]^T + R \tag{39}$$

where $L^a = 2L$, $\nu = \sqrt{L + \gamma_0}$, $w_i^{*(m)}$ and $w_i^{*(c)}$ are calculated similar to Eq. (31) with the replacement of L by L^a, Q_d is approximated by $G(\hat{x}_{k|k-1})QG^T(\hat{x}_{k|k-1})\Delta t$ where $\Delta t = t_k - t_{k-1}$

Step2 Estimation of the faults

$$\gamma_k = (y_k - \hat{y}_k) \tag{40}$$

$$N_k = (F_k^T P_{yy,k}^{-1} F_k)^{-1} F_k^T P_{yy,k}^{-1} \tag{41}$$

$$\hat{f}_k = N_k \gamma_k \tag{42}$$

$$P_k^f = (F_k^T P_{yy,k}^{-1} F_k)^{-1} \tag{43}$$

where γ_k is the innovation, $\hat{f}_k$ is the estimation of f_k and P_k^f is its error covariance matrix. N_k is the gain matrix which can achieve an unbiased estimation of f_k.

Step3 Measurement update

$$K_k = P_{xy,k} P_{yy,k}^{-1} \tag{44}$$

$$\hat{x}_{k|k} = \hat{x}_{k|k-1} + K_k(y_k - \hat{y}_k - F_k \hat{f}_k) \tag{45}$$

$$P_{k|k} = P_{k|k-1} - K_k(P_{yy,k} - F_k P_k^f F_k^T) K_k^T \tag{46}$$

This measurement update is different from that of the normal UKF [22, 27] which is given below for comparison and quick reference:

$$K_k = P_{xy,k} P_{yy,k}^{-1} \tag{47}$$

$$\hat{x}_{k|k} = \hat{x}_{k|k-1} + K_k(y_k - \hat{y}_k) \tag{48}$$

$$P_{k|k} = P_{k|k-1} - K_k P_{yy,k} K_k^T \tag{49}$$

It can be seen that the measurement update of the normal UKF, as given by Eqs. (47)-(49), does not take the fault estimation and error covariance into account. Also note that the normal UKF does not estimate the faults, which means that it does not contain Eqs. (40)-(43).

The ADS fault estimation using the RTS-UKF is shown in the following.

ADS fault estimation using the RTS-UKF

The performance of the RTS-UKF will be demonstrated under different initial conditions. The simulation data is taken from the simulation model of a Cessna Citation II aircraft. During 10 s $< t <$ 17 s. there is a 3-2-1-1 command on the aileron. The fault scenario is given in Table 1. The true initial state x_0 is as follows:

$$x_0 = [90,\ 0.056,\ 0,\ 0,\ 0.0037,\ 0]^T \tag{50}$$

First, the true initial condition (50) is used as the initial guess $\hat{x}_0$ in the filter. $P_0 = 10^{-3} \cdot I_6$. The standard deviations of the measurement noises are:

$$\sigma_{w_x} = \sigma_{w_y} = \sigma_{w_z} = 0.001 \text{ m/s}^2$$

$$\sigma_{w_p} = \sigma_{w_q} = \sigma_{w_r} = 0.000018 \text{ rad/s}$$

$$\sigma_{v_V} = 0.1 \text{ m/s},\ \sigma_{v_\alpha} = \sigma_{v_\beta} = 0.0018 \text{ rad}$$

$$\sigma_{v_\phi} = \sigma_{v_\theta} = \sigma_{v_\psi} = 0.0018 \text{ rad}$$

Therefore, Q and R can be inferred from Eqs. (9) and (10). The results are shown in Fig. 1.

The estimation errors of V, α and β, as shown in Fig. 1(a), are close to zero-mean. The estimation errors of ϕ, θ and ψ using the RTS-UKF are given in Fig. 1(b). It can be seen that the estimation errors are zero-mean except during the period when there is a maneuver (10 s $< t <$ 17

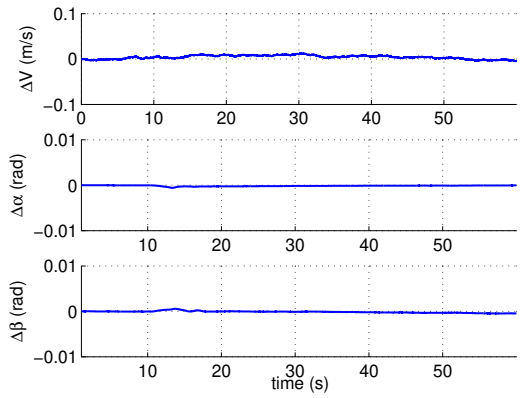

(a) Error of estimation of V, α and β

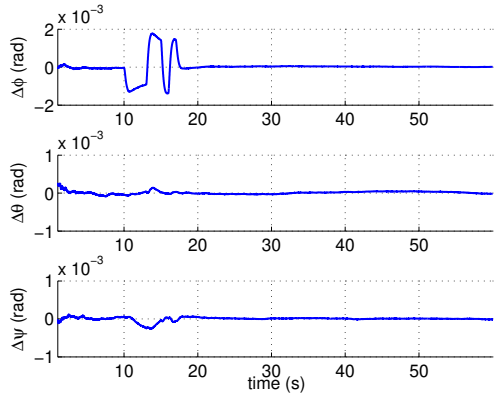

(b) Error of estimation of ϕ, θ and ψ

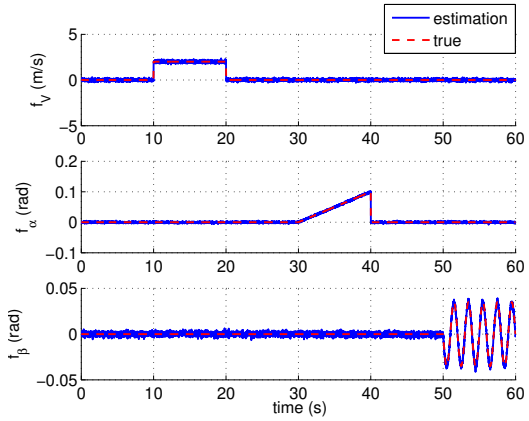

(c) Estimation of f_V, f_α and f_β

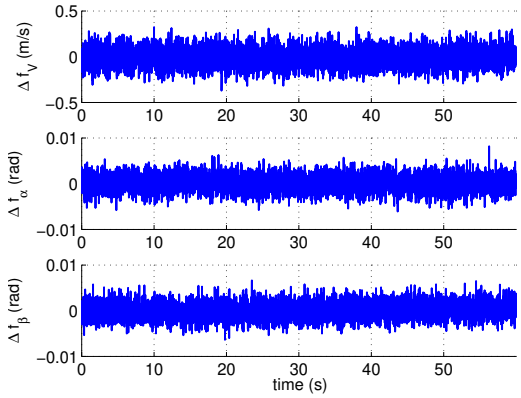

(d) Estimation error of f_V, f_α and f_β

Fig. 1: Result of state and ADS fault estimation using the RTS-UKF approach and initial condition(50) in the presence of multiple faults

s). However, during this period the estimation errors are small, e.g., the maximum estimation error of ϕ is less than $2{\times}10^{-3}$ rad.

The estimation of f_V, f_α and f_β is given in Fig. 1(c). As can be seen, all the faults are estimated in an unbiased sense. The estimation errors can be found in Fig. 1(d).

Next, the performance with two different initial conditions for $\hat{x}_0$ is tested. The two initial conditions are as follows:

$$\hat{x}_0 = [90,\ 0,\ 0,\ 0,\ 0,\ 0]^T, \tag{51}$$

$$\hat{x}_0 = [1,\ 0,\ 0,\ 0,\ 0,\ 0]^T. \tag{52}$$

The initial condition (52) significantly deviates from the true initial condition (50) whereas

condition (51) slightly deviates from condition (50). P_0 is the same with the previous simulation and is $10^{-3} \cdot I_6$.

The state estimation errors of the RTS-UKF using the initial condition Eq. (51) are shown in Fig. 2(a) and 2(b). As can be seen from Fig. 2(a), the estimation errors of V, α and β are larger than those shown in Fig. 1(a). The estimation errors of ϕ, θ and ψ, shown in Fig. 2(b), are the same as those shown in Fig. 1(b).

The state estimation errors of the RTS-UKF using the initial condition Eq. (52) are shown in Fig. 2(c) and 2(d). The estimation errors of V, α and β, shown in Fig. 2(c), are significantly worse than those shown in Fig. 1(a) and Fig. 2(a). However, the estimation errors of ϕ, θ and ψ, shown in Fig. 2(d), are still zero-mean.

The estimates of f_V, f_α and f_β using the initial condition Eqs. (51) and (52) are demonstrated in Fig. 2(e) and 2(f) respectively. As can be seen from Fig. 2(e), when the initial x_0 deviates from the true state, the estimates of the faults also deviate from their true magnitudes especially that of f_α. When the initial condition deviates significantly from the true initial condition, the performance becomes significantly worse, as can be seen in Fig. 2(f).

Based on the above simulation results, it is seen that the RTS-UKF is sensitive to the initial condition errors. This sensitivity problem will be analyzed theoretically in the following section.

B. Problem analysis of the robust three-step filter

In the previous sections, it was shown that the performance of the RTS-UKF is influenced by the given initial condition. This section analyzes the problem of the sensitivity to the initial condition.

Rewrite Eq. (45) into

$$\hat{x}_{k|k} = \hat{x}_{k|k-1} + L_k \gamma_k \tag{53}$$

where L_k is defined as

$$L_k := K_k(I - F_k N_k) \tag{54}$$

The covariance matrix $P_{xy,k}$, fault distribution matrix F_k, the innovation γ_k and x can be

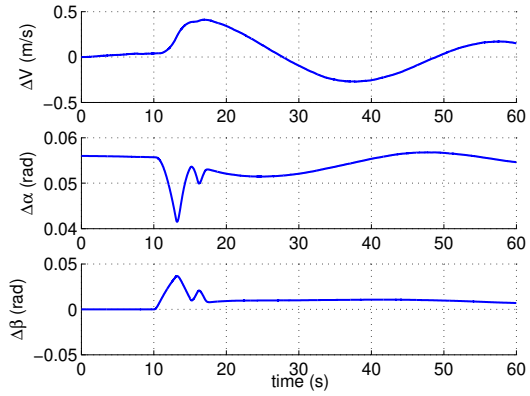

(a) Error of estimation of V, α and β using condition (51)

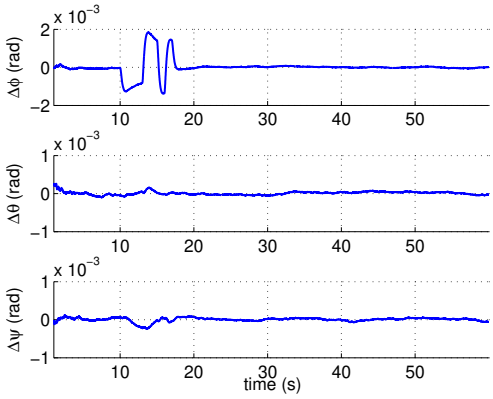

(b) Error of estimation of ϕ, θ and ψ using condition (51)

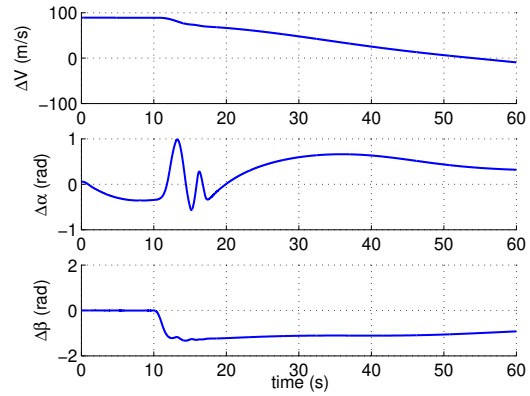

(c) Error of estimation of V, α and β using condition (52)

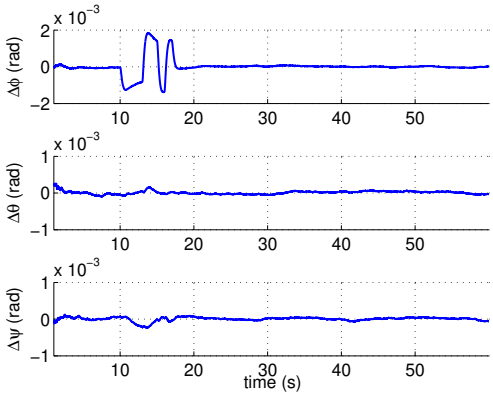

(d) Error of estimation of ϕ, θ and ψ using condition (52)

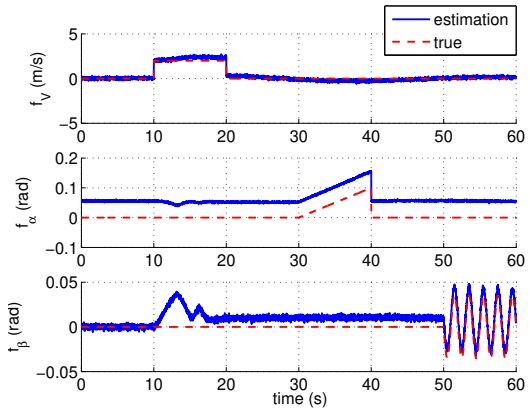

(e) Estimation of f_V, f_α and f_β using condition (51)

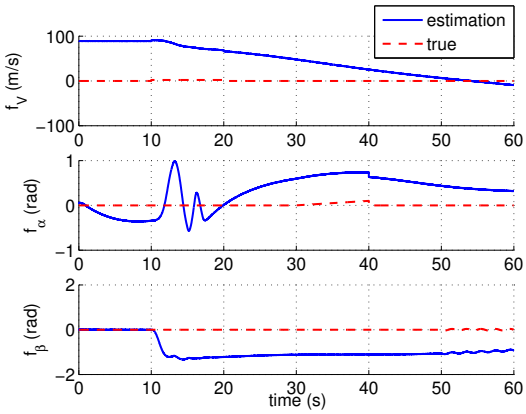

(f) Estimation of f_V, f_α and f_β using condition (52)

Fig. 2: Result of state and fault estimation using the RTS-UKF approach and two different initial conditions in the presence of multiple faults

partitioned as follows:

$$P_{xy,k} = \begin{bmatrix} P_{11} & P_{12} \\ P_{21} & P_{22} \end{bmatrix}, \quad F_k = \begin{bmatrix} I_p \\ 0 \end{bmatrix},$$
$$\gamma_k = \begin{bmatrix} \gamma_p \\ \gamma_{m-p} \end{bmatrix}, \quad x = \begin{bmatrix} x_p \\ x_{L-p} \end{bmatrix} \tag{55}$$

Since $P_{yy,k}$ is invertible, its inverse can be partitioned as follows:

$$P_{yy,k}^{-1} = \begin{bmatrix} \tilde{R}_{11} & \tilde{R}_{12} \\ \tilde{R}_{21} & \tilde{R}_{22} \end{bmatrix} \tag{56}$$

where $\tilde{R}_{11} \in \mathbb{R}^{p\times p}$, $\tilde{R}_{12} \in \mathbb{R}^{p\times(m-p)}$, $\tilde{R}_{21} \in \mathbb{R}^{(m-p)\times p}$ and $\tilde{R}_{22} \in \mathbb{R}^{(m-p)\times(m-p)}$. Therefore, Eq. (41) can be computed by

$$\begin{aligned} N_k &= [\tilde{R}_{11}^{-1}\ 0] \begin{bmatrix} \tilde{R}_{11} & \tilde{R}_{12} \\ 0 & 0 \end{bmatrix} \\ &= \begin{bmatrix} I_p & \tilde{R}_{11}^{-1}\tilde{R}_{12} \end{bmatrix} \end{aligned} \tag{57}$$

Substituting Eq. (57) into Eq. (54), it follows

$$L_k = P_{xy,k}P_{yy,k}^{-1} \begin{bmatrix} 0 & -\tilde{R}_{11}^{-1}\tilde{R}_{12} \\ 0 & I_{m-p} \end{bmatrix} \tag{58}$$

$$= \begin{bmatrix} 0 & L_{12} \\ 0 & L_{22} \end{bmatrix} \tag{59}$$

where L_{12} and L_{22} are defined as

$$L_{12} := P_{12}(\tilde{R}_{22} - \tilde{R}_{21}\tilde{R}_{11}^{-1}\tilde{R}_{12})$$
$$L_{22} := P_{22}(\tilde{R}_{22} - \tilde{R}_{21}\tilde{R}_{11}^{-1}\tilde{R}_{12})$$

Therefore, the measurement update of the robust three-step filter, denoted in Eq. (53), can be further written as follows:

$$\hat{x}_{k|k} = \hat{x}_{k|k-1} + \begin{bmatrix} L_{12}\gamma_{m-p} \\ L_{22}\gamma_{m-p} \end{bmatrix} \tag{60}$$

It can be seen that γ_p is not used in the measurement update. Since γ_p is not used, the estimation of x_p is not updated by measurements of x_p. Therefore, the estimation of $x_p(V,\ \alpha$ and $\beta)$, is sensitive to the initial condition. If the initial x_0 significantly deviates from the true value, it will not be corrected to the true value. However, the estimation of ϕ, θ and ψ is not influenced since they are updated by the measurement. This is consistent with the result shown in Figs. 2(b) and 2(d), where the estimation of ϕ, θ and ψ is still good even when that of V, α and β is not.

In case that $p = m$ and rank $F_k = m$, it can be found that

$$N_k = F_k^{-1} \tag{61}$$

$$L_k = 0 \tag{62}$$

Consequently, the measurement update of the three-step Kalman filter is

$$\hat{x}_{k|k} = \hat{x}_{k|k-1} \tag{63}$$

This means that all the states are not updated by their measurements. In this situation, all the state estimation will be sensitive to the initial condition.

Through the analysis in this section and the performance demonstration of the RTS-UKF in Section III A, the need for a modification of the RTS-UKF is emphasized. In real life, the exact initial condition is difficult to obtain due to uncertainties in the system (which can also be found in Section V). The RTS-UKF will interpret the initialization error as a fault, which results into wrong fault estimation. Therefore, the RTS-UKF can not be applied to the FDD of the ADSs.

C. Novel Adaptive Three-Step Unscented Kalman Filter for ADS FDD

Having found the cause for performance degradation of the RTS-UKF, this section proposes a novel ATS-UKF to solve the ADS FDD. The sensitivity to the initial condition of the RTS-UKF can be solved by performing the measurement update of normal UKF.

It should be noted that the RTS-UKF only considers the estimation of the faults. It does not detect and isolate the faults. The proposed ATS-UKF deals with not only the estimation of the faults, but also the detection and isolation.

In the following, the initial measurement update and FDI scheme are introduced. Then the complete FDD system is introduced.

1. Initial measurement update

The solution to reduce the sensitivity of the RTS-UKF to the initial condition is proposed in this subsection, which is to use the measurement update of normal UKF (Eqs. (47)-(49)) when the state estimation is influenced by the initialization error. However, when the correction is sufficient, i.e., when the measurement update of the UKF is sufficient, needs to be determined. This paper proposes a criteria which can determine whether the measurement update of the UKF is sufficient. The details are given as follows:

Let $C_{ii,k}$, $i = 1, 2, 3$ denote the ith diagonal elements of the innovation covariance matrix C_k associated with the measurements which are not used in the update of the RTS-UKF at time step k. (i.e., the measurement of V, α and β respectively in this paper).

Define the change of the innovation variance $\Delta C_{ii,k}$ as

$$\Delta C_{ii,k} := C_{ii,k} - C_{ii,k-1}, \quad i = 1, 2, 3. \tag{64}$$

When the following inequality holds, the measurement update can be regarded as sufficient. The inequality is

$$\Delta C_{ii,k} < \eta_i, \quad i = 1, 2, 3. \tag{65}$$

where η_i, $i = 1, 2, 3$ are pre-defined constants which can be tuned to stop the measurement update. The principle is that if there are initialization errors, $C_{ii,k}$ is not constant. When the filter achieves steady-state, $C_{ii,k}$ is approximately constant. Therefore, $\Delta C_{ii,k}$ should be small. If $\Delta C_{ii,k}$ is smaller than η_i, then it indicates that the filter has reached steady-state and the measurement update of the UKF is sufficient. If η_i is chosen to be small, then the number of initial measurement update will be bigger while the influence of the initial condition error will be less. C_k can be estimated using the following [29, 30]:

$$\hat{C}_k = \frac{1}{N} \sum_{j=k-N+1}^{k} \gamma_j \gamma_j^T \tag{66}$$

where γ_j denotes the innovation at time step j.

2. Fault Detection and Isolation

The fault detection is performed by monitoring the innovation variance of the filter. In the presence of ith fault, $C_{ii,k}$ increases. The fault detection and isolation logic at time step k is:

if $C_{ii,k} > T_i$, $F_{A_i} = 1$. otherwise $F_{A_i} = 0$, i = 1,2,3.

where $F_A = [F_{A_V}\ F_{A_\alpha}\ F_{A_\beta}]^T$ are the alarm indicators. T_i are the thresholds which are designed to detect the faults in the V, α and β sensors respectively. These thresholds are designed based on the fault-free case. It can be seen that the fault detection and isolation are simultaneously realized.

The weighted fault estimation can be calculated as follows:

$$\bar{f}_{i,k} = F_{A_i}\hat{f}_{i,k}, \qquad i = 1, 2, 3. \tag{67}$$

3. Adaptive Three-Step Unscented Kalman Filter

When the initial measurement update is sufficient, there are two options to achieve FDD which are as follows:

1. After the initial measurement update, the FDI scheme is used to detect and isolate the faults. The RTS-UKF is used to estimate the faults.

2. After the initial measurement update, the FDI scheme is used to detect and isolate the faults. If there are no faults detected, the UKF is used and the fault estimation is considered to be zero. If there are faults detected, then the RTS-UKF is used for the fault estimation and measurement update.

The ATS-UKF proposed in this paper, is based on the latter one since it can reduce the computational load. The measurement update of the ATS-UKF switches adaptively between that of the normal UKF and that of the RTS-UKF through the FDI scheme. The specific three steps of the ATS-UKF are given as follows:

1. Time update

   This is the same as in the UKF, which also includes the sigma point calculation. The steps are described by Eqs. (30)- (39).

2. Fault estimation

   Before estimating the faults, the FDI, which has been introduced above, is performed. If $F_A = 0$, then $\hat{f}_k = 0$. If $F_A \neq 0$, then the faults are estimated using the RTS-UKF, which is described by Eqs. 40-(43). This step is the FDD.

3. Measurement update

   As mentioned, during the initial measurement update, the measurement update of the normal UKF is applied. When the initial measurement update is done, the measurement update of the ATS-UKF is as follows:

   (a) If $F_A = 0$, use the the measurement update of the normal UKF.

   In this situation, there are no faults detected in the system. To reduce the computational load, the measurement update of the UKF is used. This means that the faults are considered to be zero, so that the faults estimation and measurement update of the RTS-UKF are not needed. The steps are described by Eqs. (47)-(49).

   (b) If $F_A \neq 0$, use the measurement update of the RTS-UKF.

   In this situation, faults are detected. Therefore, the measurement update of the RTS-UKF is needed to obtain an unbiased state estimation and fault estimation, which can not be achieved using the normal UKF. The steps are described by Eqs. (44)-(46).

D. ADS FDD using the ATS-UKF

In this section, the FDD as well as the state estimation performance of the proposed ATS-UKF is demonstrated using two different fault scenarios. The initial condition is the same as in Eq. (52). The threshold to stop the initial measurement update is $\eta = [5 \times 10^{-3},\ 2 \times 10^{-5},\ 2 \times 10^{-5}]^T$ and the threshold to detect the fault is $T = [0.2,\ 1 \times 10^{-4},\ 5 \times 10^{-5}]^T$.

1. Multiple FDD

In this scenario, consecutive ADS faults are generated, which are shown in Table 1. The results using the ATS-UKF are shown in Fig. 3.

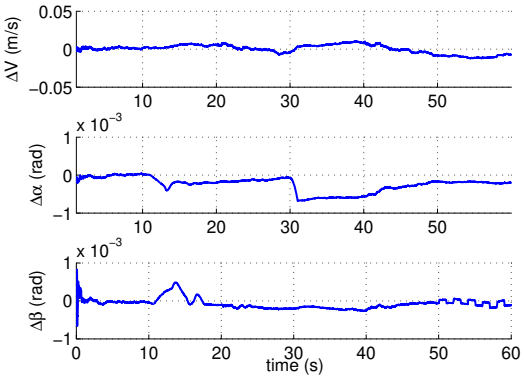

(a) Error of estimation of V, α and β

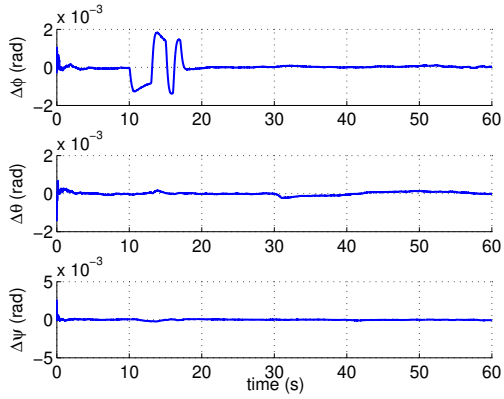

(b) Error of estimation of ϕ, θ and ψ

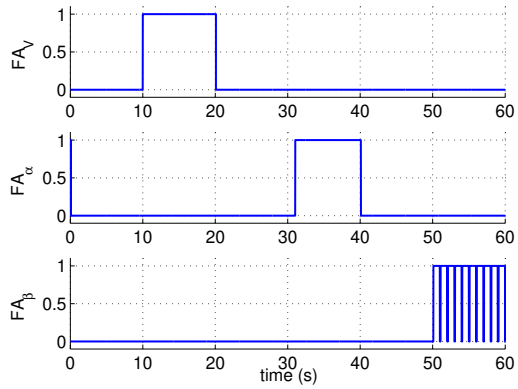

(c) Fault detection and isolation

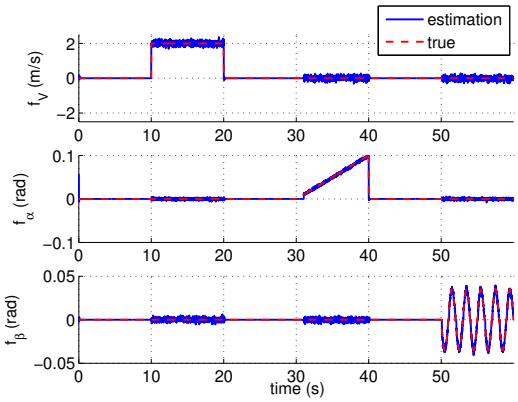

(d) Estimation of f_V, f_α and f_β

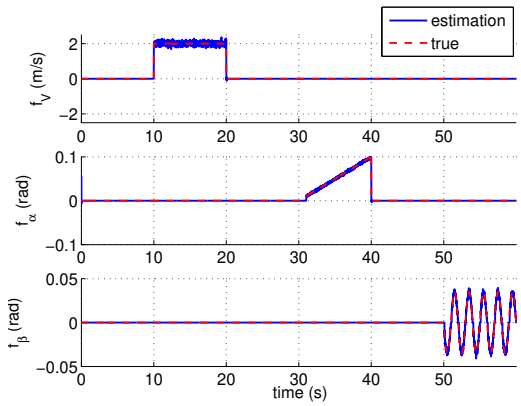

(e) Weighted estimation of f_V, f_α and f_β

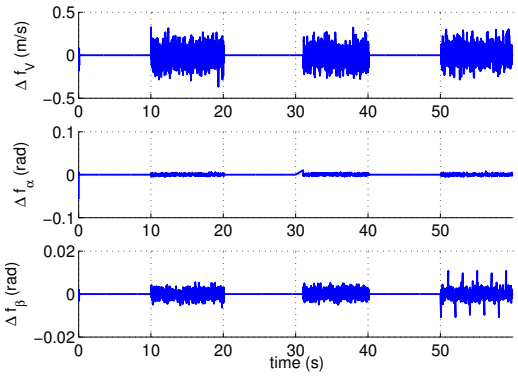

(f) Error of estimation of f_V, f_α and f_β

Fig. 3: Result of state estimation and ADS FDD using the proposed ATS-UKF approach in the presence of multiple faults

It is found that using the above thresholds, the initial measurement update is only performed for

two time steps. The estimation of V, α and β is shown in Fig. 3(a). Despite the fact that the initial x_0 significantly deviates from the true state, the estimation is still satisfactory. This means that the sensitivity to the initial condition of the RTS-UKF is tackled by the ATS-UKF. The estimation of ϕ, θ and ψ, as shown in Fig. 3(b), is also satisfactory. This demonstrates the state estimation performance of the ATS-UKF.

The fault detection and isolation is achieved by checking F_{A_V}, F_{A_α} and F_{A_β}, which is shown in Fig. 3(c). From the figure, it can be seen that f_V is detected instantaneously. The detection of f_α takes longer than that of f_V. This is because f_α is a drift fault which is a slow time-varying fault. f_β is also detected instantaneously. However, F_{A_β} switches from 1 to 0 nine times. This is as expected since the oscillatory fault crosses zero nine times. When the magnitude of the fault is zero, it can be regarded as no fault. From the figure, it is obvious that fault isolation is also achieved. For instance, when $F_{A_V} = 1$, both F_{A_α} and F_{A_β} are equal to zero, which means only f_V occurs.

The estimation of f_V, f_α and f_β is shown in Fig. 3(d). As can be seen, all the faults are estimated in an unbiased sense. The weighted fault estimation, calculated using Eq. (67), is shown in Fig. 3(e). The error of the estimation of f_V, f_α and f_β is shown in Fig. 3(f). It is seen that all the estimation errors are zero-mean. This demonstrates the fault estimation performance of the ATS-UKF. It is also noticed that when there are no faults or the faults are not detected, the estimates of the fault are zero and so are the estimation errors. This is due to the fact that when there are no faults detected, the measurement update of the UKF is used and the faults are considered to be zero.

The fault detection of the oscillatory faults, shown in Fig. 3(c), shows a chattering behavior. To detect the presence of oscillatory failures, the detection logic of oscillatory faults in Goupil [31] is used. The basic idea is to count the crossings of the fault estimate (shown in Fig. 3(e)) through a positive and negative threshold within a sliding time window. In this paper, the oscillatory faults are detected if one full oscillation is detected. The result of detecting the oscillatory fault is shown in Fig. 4(a). In the figure, OFC denotes oscillatory failure case (OFC). As can be seen, an oscillatory fault is only detected in the β sensor. If we take the bigger value of F_{Ai} and OFC_i (i is associated with the sensor of V, α and β), the fault detection including the detection of the oscillatory fault can be obtained, which is demonstrated in Fig. 4(b). In the figure, the red dashed line indicates

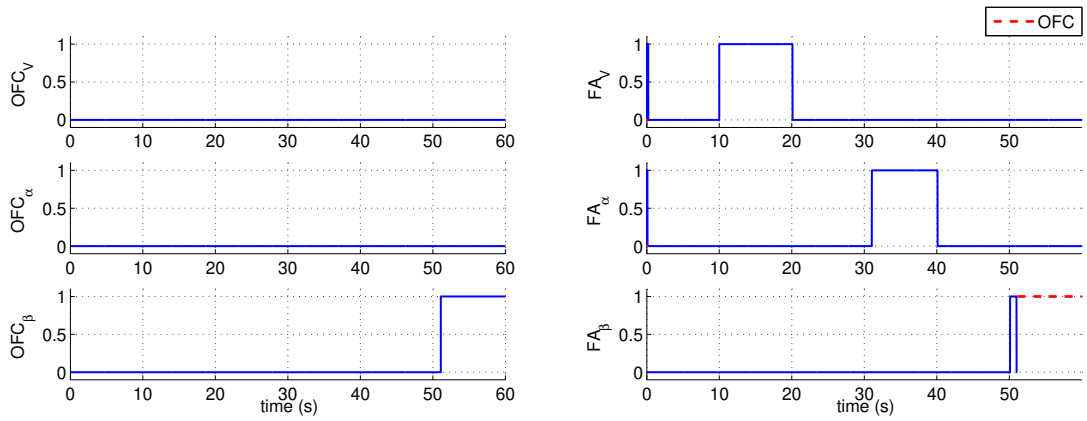

(a) Detection of oscillatory faults, *OFC* indicates the detection of oscillatory faults

(b) Fault detection and isolation including oscillatory fault indication

Fig. 4: Result of fault detection and isolation using the proposed ATS-UKF approach in the presence of multiple faults

that the detected fault is an oscillatory fault.

2. Simultaneous FDD

In this scenario, simultaneous faults are generated which are shown in Table 2. The ATS-UKF is used to detect, isolate and estimate these faults. The results are given in Fig. 5.

The estimation of V, α, β and ϕ, θ and ψ using the ATS-UKF is shown in Fig. 5(a) and Fig. 5(b), respectively. As can be seen, even in the presence of simultaneous faults, the state estimation performance of the ATS-UKF is still satisfactory.

The fault detection and isolation performance is shown in Fig. 5(c). As can be seen, there are no false alarms, which demonstrates its good performance. For the detection of f_α and f_β during 10 s$< t <$ 20 s, and f_V during 30 s$< t <$ 40 s, there are detection delays since there are drift faults. The red dashed lines in the figure indicate that the detected faults are oscillatory faults.

Fig. 5(d) and 5(e) show the estimation and weighted estimation of f_V, f_α and f_β, respectively. It can be seen that the fault estimation performance is satisfactory. All faults are estimated in an unbiased sense including the oscillatory faults. The estimation error of f_V, f_α and f_β is shown in Fig. 5(f). It can be seen that the error is zero-mean, which confirms the good estimation performance

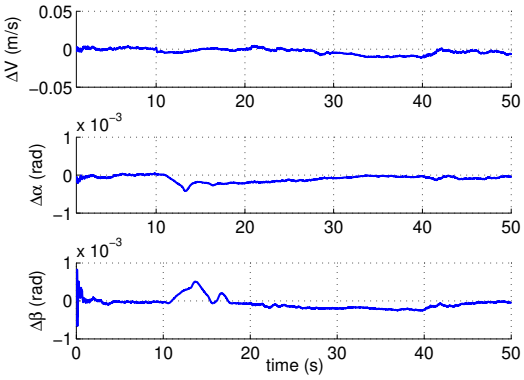

(a) Error of estimation of V, α and β

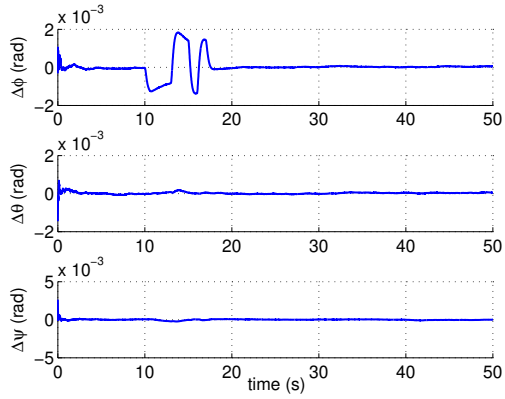

(b) Error of estimation of ϕ, θ and ψ

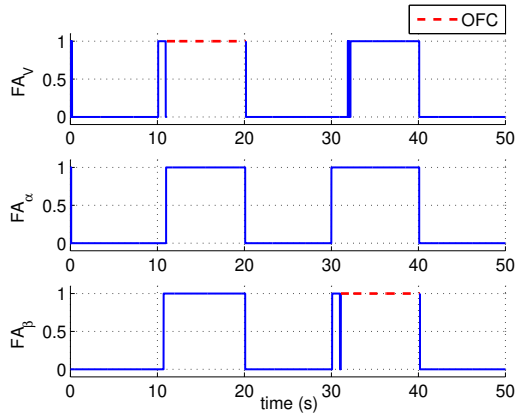

(c) Fault detection and isolation

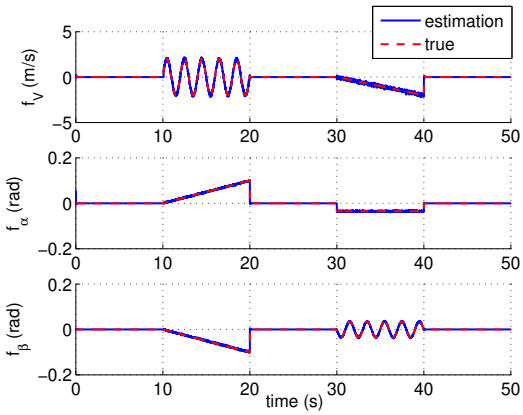

(d) Estimation of f_V, f_α and f_β

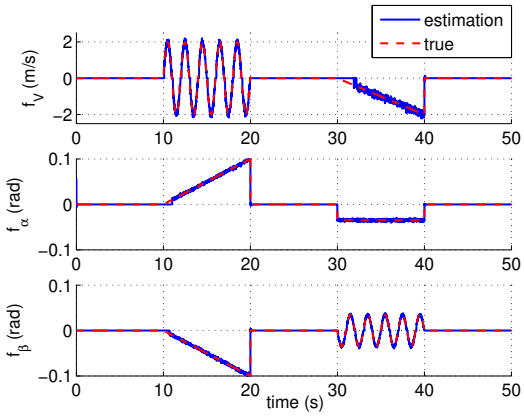

(e) Weighted estimation of f_V, f_α and f_β

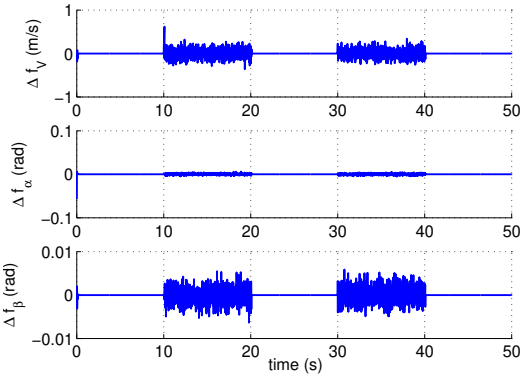

(f) Error of estimation of f_V, f_α and f_β

Fig. 5: Result of state and ADS FDD using the proposed ATS-UKF approach in the presence of simultaneous faults

of the ATS-UKF.

IV. Performance validation using real flight data

In the previous section, the FDD performance of the ATS-UKF is tested using simulated aircraft data. In this section, the FDD performance of the ATS-UKF is validated using real flight test data of the Cessna Citation II aircraft. Air data information such as α and β are measured for post flight analysis. The real flight data contains uncertainties such as biases and spikes. Additionally, in real flight, external disturbances, such as changing wind, can also influence the air data measurements. Therefore, the real flight data poses challenges to the ADS FDD problem and provides a realistic validation of the performance of FDD approaches such as the ATS-UKF.

The primary objective of the flight test is aerodynamic model identification where a number of maneuvers were performed by the aircraft in order to obtain sufficient excitation. Since there were no faults during the flight, sensor faults are injected into the real flight data to validate the FDD performance of the ATS-UKF. Besides the fault scenarios presented in Tables 1 and 2, a fault-free case is also studied.

The real flight data used in this paper is the same as that in Lu et. al [26]. In Lu et. al, the estimated wind turns out to be time varying. This can test the ADS FDD performance of the ATS-UKF under the condition of winds.

The update rates of the on-board sensors are given in Table 3.

Table 3: Update frequencies of different measurements

Measurements	Unit	Update frequency
V	[m/s]	100 Hz
u_n, v_n, w_n	[m/s]	1 Hz
α, β	[rad]	100 Hz
ϕ, θ	[rad]	100 Hz
ψ	[rad]	10 Hz

A. Real-life measurement model

For simulated aircraft data, the measurement model is given in Eqs. (19) - (24). If $f = 0$, the measurements are only corrupted by white Gaussian noises, as can be seen from the equations.

However, this is never the case in real life. In this flight test, the air data information, such as α and β, is measured by multiple vanes on a boom (shown in Fig. 6) which is mounted on the nose of the aircraft. The angle of attack and angle of sideslip measured by the vanes are denoted by α_{vm} and β_{vm}, respectively. The measurements α_{vm} and β_{vm} is different from Eqs. (20) and (21), respectively. The measurement model for the real-life measurements is given as follows [32–34]:

$$V_m = V + v_V \tag{68}$$

$$\alpha_m = C_{\alpha 0} + (1 + C_{up})\alpha + \frac{x_\alpha q}{V} + v_\alpha \tag{69}$$

$$\beta_m = C_{\beta 0} + (1 + C_{si})\beta - \frac{x_\beta r}{V} + \frac{z_\beta p}{V} + v_\beta \tag{70}$$

$$\phi_m = \phi + v_\phi \tag{71}$$

$$\theta_m = \theta + v_\theta \tag{72}$$

$$\psi_m = \psi + v_\psi \tag{73}$$

where x_α, x_β and z_β are the position of the vanes in the body frame, $C_{\alpha 0}$, $C_{\beta 0}$, C_{up} and C_{si} are the boom correction parameters. In this paper, z_β is assumed to be zero. The parameter estimation can be found in Lu et al. [34]. For the ADS FDD using real flight data, this measurement model is used. However, it should be noted that in this real-life measurement model, boom bending is considered to be negligible for the maneuvers flown.

Fig. 6: The vanes on the boom for measuring the angle of attack and angle of sideslip. Photo credits by Daan Pool.

B. ADS FDD using real flight data in the absence of faults

Using the real-life measurements, uncertainties and disturbances such as varying winds can also have a negative influence on the FDD performance, which can result in false alarms. Under this condition, the FDD approaches should not give false alarms. In this section, the ATS-UKF is tested in a fault-free case to verify whether it gives false alarms.

In order to show the effectiveness of the ATS-UKF, the RTS-UKF is also applied to estimate the ADS faults. The initial condition x_0 given for the RTS-UKF is the first measurement which is:

$$[104.8733,\ 0.0796,\ 0.0073,\ -0.0019,\ 0.0733,\ 4.6692]^T \tag{74}$$

The initial condition x_0 given for the ATS-UKF is:

$$[1,\ 0,\ 0,\ 0,\ 0,\ 0]^T \tag{75}$$

In this manner, the initial condition given for the RTS-UKF is close to the true state whereas that of the ATS-UKF significantly deviates from the true state. The threshold to stop the initial measurement update is $\eta = [5 \times 10^{-3},\ 2 \times 10^{-5},\ 2 \times 10^{-5}]^T$ and the threshold to detect the fault is $T = [0.2,\ 1 \times 10^{-4},\ 5 \times 10^{-5}]^T$, which are the same as those used in the previous section.

The estimation of V, α and β using the RTS-UKF is given in Fig. 7(a). The fault estimation using the RTS-UKF is given in Fig. 7(b). As can be seen, the estimated faults deviate from their true magnitudes. This result shows that the RTS-UKF is not able to be applied for real applications unless modifications are made.

The results of the ATS-UKF are shown in Figs. 7(c) - 7(f). The estimation of V, α and β, and ϕ, θ and ψ are shown in Fig. 7(c) and 7(d) respectively. The estimates of α and β using the ATS-UKF are different from those using the RTS-UKF. The fault detection result, shown in Fig. 7(e), indicates that there are no faults. This demonstrates that the ATS-UKF does not give false alarms in the presence of no faults even when the real flight data is used. The weighted estimates of f_V, f_α and f_β, shown in Fig. 7(f), are zero-mean. This confirms the fault estimation performance of the ATS-UKF.

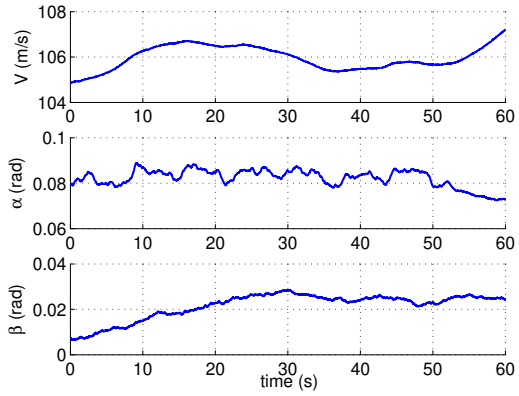

(a) Estimation of V, α and β using the RTS-UKF

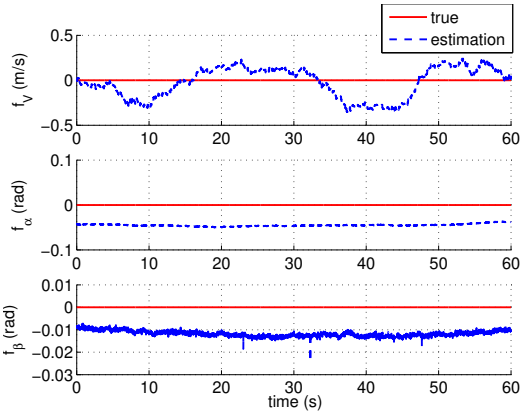

(b) Estimation of f_V, f_α and f_β using the RTS-UKF

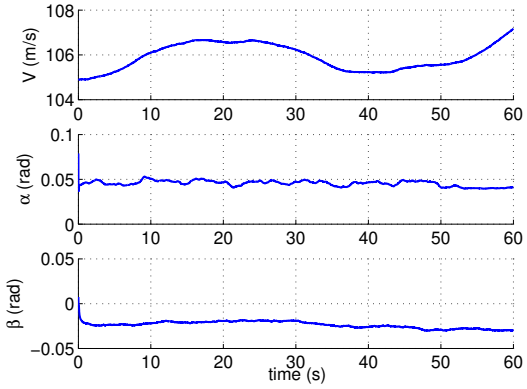

(c) Estimation of V, α and β using the ATS-UKF

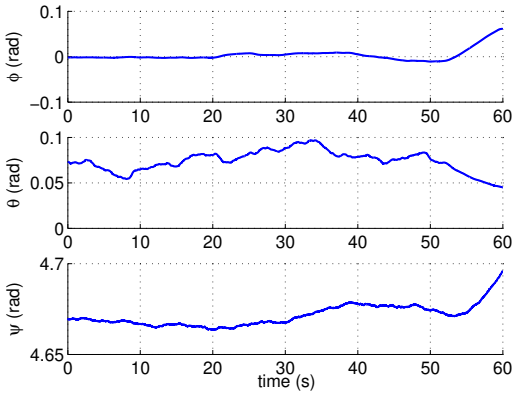

(d) Estimation of ϕ, θ and ψ using the ATS-UKF

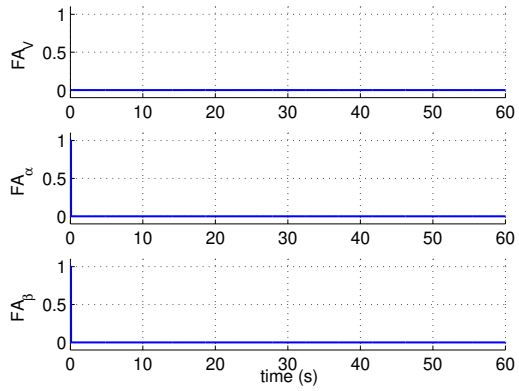

(e) Fault detection and isolation using the ATS-UKF

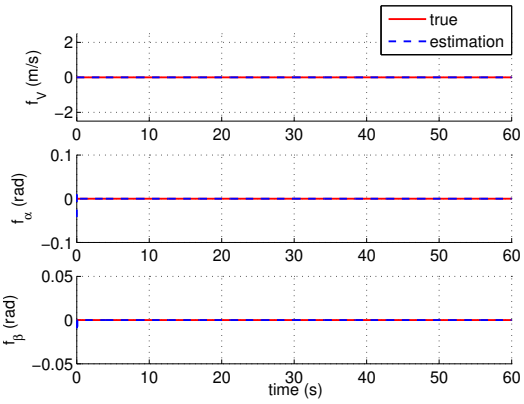

(f) Weighted estimation of f_V, f_α and f_β using the ATS-UKF

Fig. 7: State estimation and ADS FDD of the real-life measurement model of the aircraft using the RTS-UKF and the ATS-UKF approach in the absence of faults

C. ADS FDD using real flight data in the presence of multiple faults

In this subsection, the ADS FDD performance of the ATS-UKF will be verified using the real-life measurement model in the presence of multiple faults (given in Table 1). The initial condition for RTS-UKF is the same as in (74) and that of the ATS-UKF is the same as in (75).

The results using these two approaches are shown in Fig. 8.

The estimation of V, α and β using the RTS-UKF is shown in Fig. 8(a). The fault estimation is shown in Fig. 8(b). Although the initial condition of the RTS-UKF is chosen to be the measurements, the estimation of the faults are still biased. This shows the drawback of the RTS-UKF when it is used in practice because the initial condition error will be estimated as a bias fault.

The estimation of V, α, β and ϕ, θ, ψ using the ATS-UKF is presented in Fig. 8(c) and 8(d) respectively. It can be seen that the estimates of α, β are again different from those of the RTS-UKF shown in Fig. 8(a).

The fault detection and isolation using the ATS-UKF is given in Fig. 8(e). No false alarms are generated and the isolation is also correct. It can be seen that the performance is as good as that in Fig. 4(b) where the simulation data is used. The oscillatory fault is also detected, which is shown by the red dashed line.

The weighted estimation of f_V, f_α and f_β using the ATS-UKF is presented in Fig. 8(f). Even though the initial condition of the ATS-UKF deviates from the true state significantly, its performance is not sensitive to the initial condition. Since the faults are estimated in an unbiased sense, the estimates of α, β using the ATS-UKF are more reliable than those using the RTS-UKF.

D. ADS FDD using real flight data in the presence of simultaneous faults

In this subsection, simultaneous faults (given in Table 2) are injected into the real flight data to validate the performance of the ATS-UKF. The result of the RTS-UKF is also presented, which is given in Fig. 9. From this figure, it is seen the fault estimation of the RTS-UKF is again biased although the initial x_0 is chosen to be the measurements. This highlights the limitation of the RTS-UKF when used in reality.

The results using the ATS-UKF is shown in Fig. 10. The state estimation is presented in

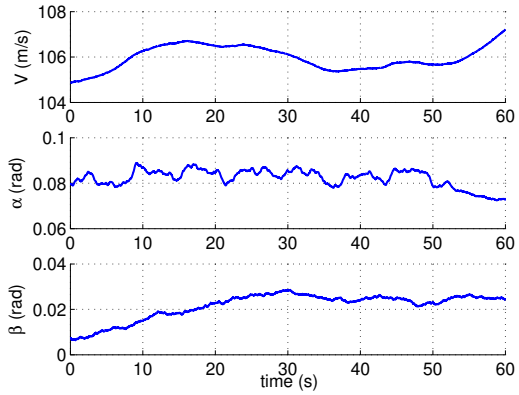

(a) Estimation of V, α and β using the RTS-UKF

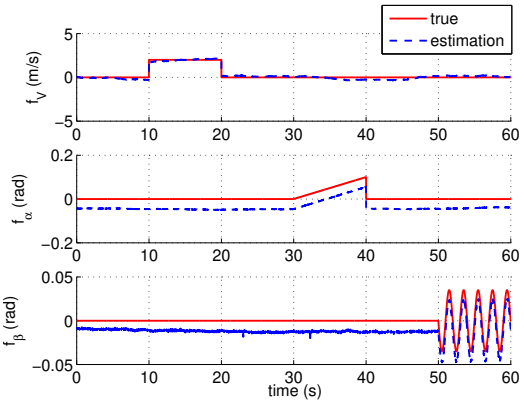

(b) Estimation of f_V, f_α and f_β using the RTS-UKF

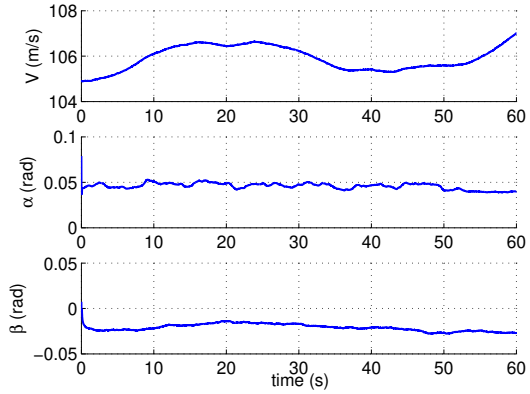

(c) Estimation of V, α and β using the ATS-UKF

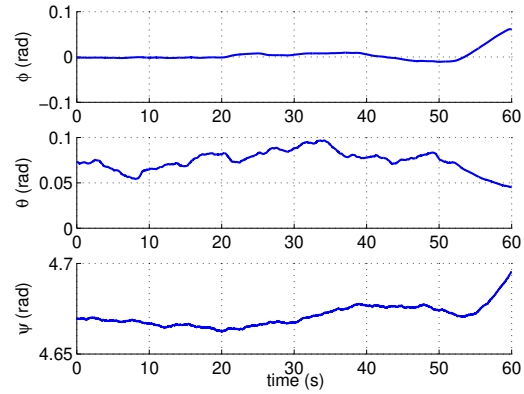

(d) Estimation of ϕ, θ and ψ using the ATS-UKF

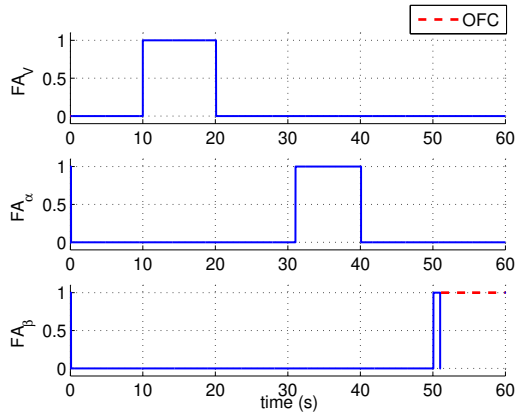

(e) Fault detection and isolation using the ATS-UKF

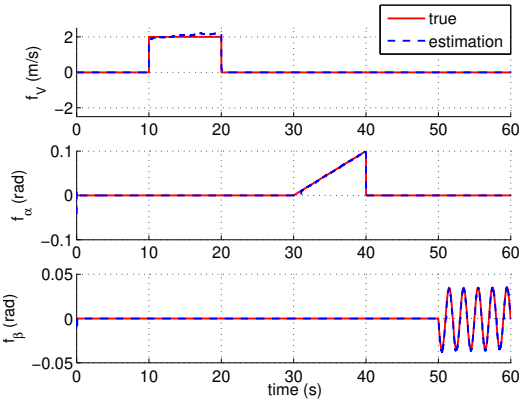

(f) Weighted estimation of f_V, f_α and f_β using the ATS-UKF

Fig. 8: State estimation and ADS FDD of the real-life measurement model of the aircraft using the RTS-UKF and the ATS-UKF approach in the presence of multiple faults

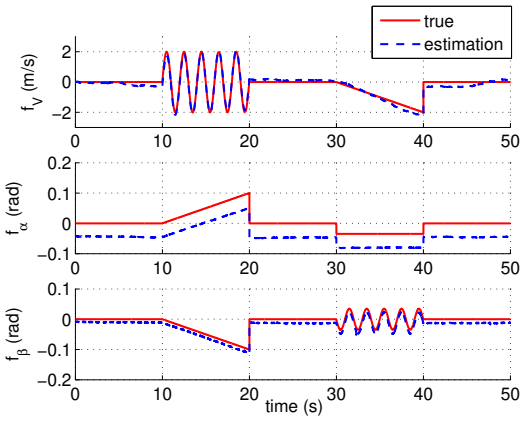

(a) Estimation of f_V, f_α and f_β

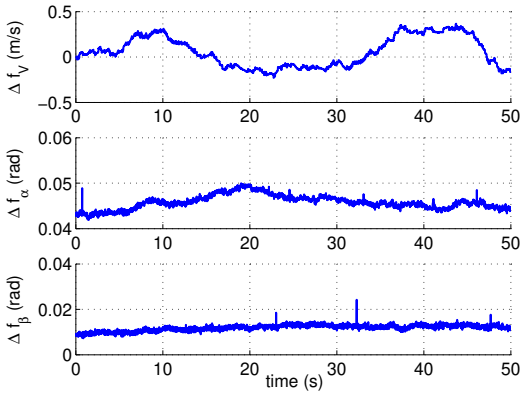

(b) Error of estimation of f_V, f_α and f_β

Fig. 9: ADS FDD of the real-life measurement model of the aircraft using the RTS-UKF approach in the presence of simultaneous faults

Fig. 10(a) and 10(b) respectively.

The fault detection and isolation using the ATS-UKF is shown in Fig. 10(c). No false alarms are observed from the figure and the oscillatory faults are also detected. The performance is as good as that in Fig. 5(c) where the simulation data is used. This confirms the FDI performance of the ATS-UKF.

Estimation and weighted estimation of f_V, f_α and f_β using the ATS-UKF are shown in Fig. 10(d) and 10(e), respectively. All fault estimates achieve an unbiased estimation. The fault estimation errors are demonstrated in Fig. 10(f). Although the errors are not zero-mean, they are small compared to the states.

V. Conclusions

This paper deals with the Air Data Sensor (ADS) Fault Detection and Diagnosis (FDD) of aircraft. First, the Robust Three-Step Kalman Filter (RTS-KF) is extended to the Robust Three-Step Unscented Kalman Filter (RTS-UKF) to cope with nonlinear systems. Second, the RTS-UKF is found to be sensitive to the initial condition. The problem is analyzed theoretically and subsequently, a novel Adaptive Three-Step Unscented Kalman Filter (ATS-UKF) is proposed to detect, isolate and estimate the ADS faults. The ATS-UKF contains three steps: time update, fault estimation

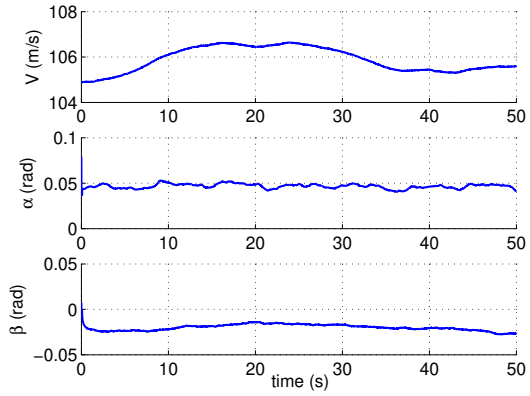

(a) Estimation of V, α and β

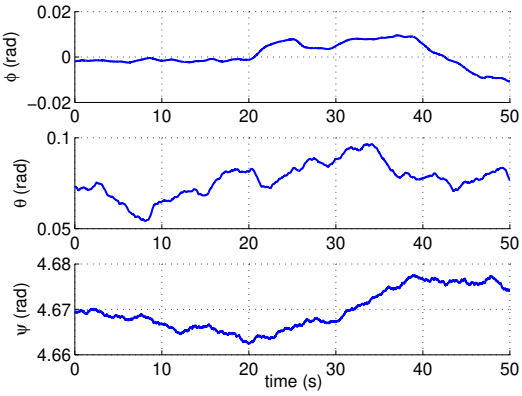

(b) Estimation of ϕ, θ and ψ

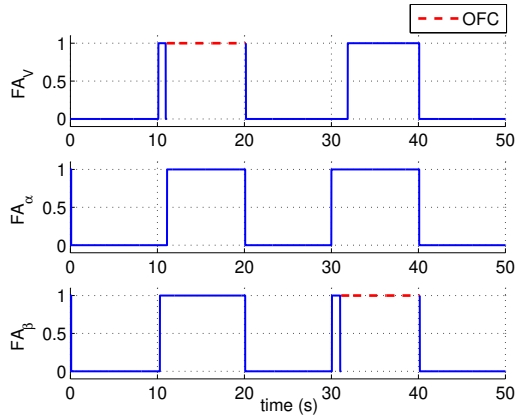

(c) Fault detection and isolation

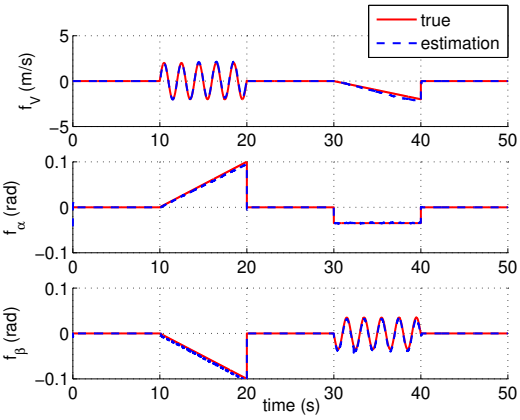

(d) Estimation of f_V, f_α and f_β

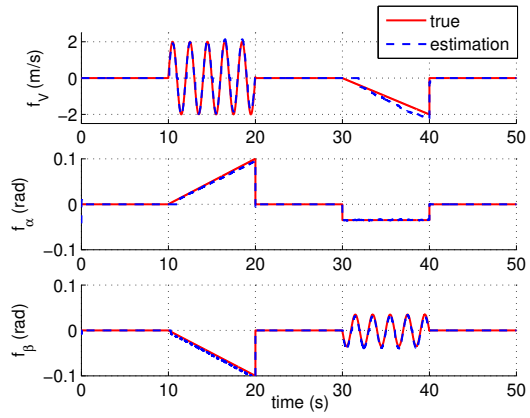

(e) Weighted estimation of f_V, f_α and f_β

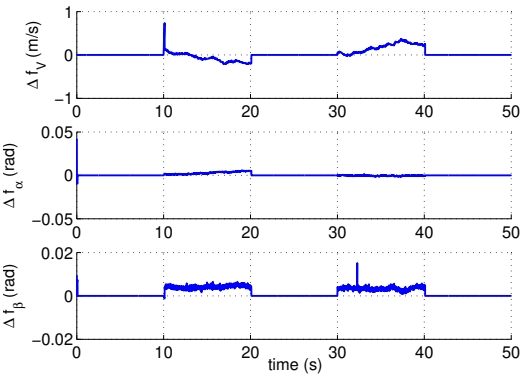

(f) Error of estimation of f_V, f_α and f_β

Fig. 10: State estimation and ADS FDD of the real-life measurement model of the aircraft using the ATS-UKF in the presence of simultaneous faults

and measurement update. The ATS-UKF is validated using simulated aircraft data, which shows

good FDD performance.

The performance of the ATS-UKF is further validated using real flight data of the Cessna Citation II aircraft to test its performance under real-life uncertainties. It was found that although the measurement data contains biases which can not be removed completely and the initial condition is far from the true state, the ATS-UKF is still able to maintain its satisfactory FDD performance. This demonstrates that it can be applied in practice.

This ATS-UKF, which deals with ADS FDD, can be incorporated into Fault Tolerant Control (FTC) systems to further enhance the safety of the aircraft. It can detect faults without giving false alarms. In addition, it can provide both unbiased state estimation and fault estimation, which are important for the recovery from sensor faults.

In the future, the ATS-UKF should be integrated into a FTC system. Finally, it is highly recommended that a real-world flight experiment is designed and executed to detect and estimate ADS faults in aircraft during flight.

References

1. Patton RJ. Fault-tolerant Control Systems: The 1997 Situation. In: *Proc. of IFAC Symp. on Fault Detection, Supervision and Safety for Technical Processes.* IFAC, Laxenburg, Austria; 1997:1033–54.
2. Chen J, Patton RJ. Robust Model-based Fault Diagnosis for Dynamic Systems. Norwell, MA, USA: Kluwer Academic Publishers; 1999:19–21. ISBN 0-7923-8411-3.
3. Isermann R. Model-based Fault-Detection and Diagnosis- Status and Applications. *Annual Reviews in Control* 2005;29(1):71–85. doi:10.1016/j.arcontrol.2004.12.002.
4. Venkatasubramanian V, Rengaswamy R, Yin K. A Review of Process Fault Detection and Diagnosis Part I : Quantitative model-based methods. *Computers and Chemical Engineering* 2003;27:293–311. doi:10.1016/S0098-1354(02)00160-6.
5. Marzat J, Piet-Lahanier H, Damongeot F, Walter E. Model-based Fault Diagnosis for Aerospace Systems: a Survey. *Proceedings of the Institution of Mechanical Engineers, Part G: Journal of Aerospace Engineering* 2012;226(10):1329–60. doi:10.1177/0954410011421717.
6. Hajiyev C, Caliskan F. Fault Diagnosis and Reconfiguration in Flight Control Systems. Boston: Kluwer Academic Publishers; 2003.
7. Hajiyev C, Soken HE. Robust Adaptive Kalman Filter for Estimation of UAV Dynamics in

the Presence of Sensor/Actuator Faults. *Aerospace Science and Technology* 2013;28(1):376–83. doi:10.1016/j.ast.2012.12.003.

8. Goupil P. AIRBUS State of the Art and Practices on FDI and FTC in Flight Control System. *Control Engineering Practice* 2011;19(6):524–39. doi:10.1016/j.conengprac.2010.12.009.
9. Zolghadri A. Advanced Model-based FDIR Techniques for Aerospace Systems: Today Challenges and Opportunities. *Progress in Aerospace Sciences* 2012;53:18–29. doi:10.1016/j.paerosci.2012.02.004.
10. Zolghadri A, Henry D, Cieslak J, Efimov D, Goupil P. Fault Diagnosis and Fault-Tolerant Control and Guidance for Aerospace Vehicles, From Theory to Application. Springer, Series: Advances in Industrial Control; 2013:1–22. ISBN 9781447153122.
11. Houck D, Atlas L. Air Data Sensor Failure Detection. In: *17th Digital Avionics Systems Conference, AIAA/IEEE/SAE*. 1. ISBN 0780350863; 1998:1–8.
12. Freeman P, Seiler P, Balas GJ. Air Data System Fault Modeling and Detection. *Control Engineering Practice* 2013;21(10):1290–301. doi:10.1016/j.conengprac.2013.05.007.
13. Eubank RD, Atkins EM, Ogura S. Fault Detection and Fail-Safe Operation with a Multiple-Redundancy Air-Data System. In: *AIAA Guidance, Navigation and Control Conference*. AIAA 2010-7855; Toronto, Ontario Canada; 2010:1–14.
14. Lombaerts T. Fault Tolerant Flight Control- A Physical Model Approach. Ph.D. thesis; Delft University of Technology; 2010.
15. Ellsworth JC, Whitmore SA. Reentry Air Data System for a Sub-orbital Spacecraft Based on X-34 Design. In: *AIAA Aerospace Sciences Meeting and Exhibit*. AIAA 2007-1200; Reno, Nevada; 2007:1–31.
16. Rohloff TJ, Whitmore SA, Catton I. Fault-Tolerant Neural Network Algorithm for Flush Air Data Sensing. *Journal of Aircraft* 1999;36(3):541–9. doi:10.2514/2.2489.
17. Nebula F, Palumbo R, Morani G, Corraro F. Virtual Air Data System Architecture for Space Reentry Applications. *Journal of Spacecraft and Rockets* 2009;46(4):818–28. doi:10.2514/1.42485.
18. Nebula F, Palumbo R, Morani G. Virtual Air Data : a Fault-Tolerant Approach Against ADS Failures. In: *AIAA Guidance, Navigation and Control and Co-located Conferences*. Boston, MA; 2013:1–14.
19. Looye G, Joos HD. Design of Robust Dynamic Inversion Control Laws using Multi-Objective Optimization. In: *AIAA Guidance, Navigation and Control Conferences and Exhibit*. AIAA-2001-4285; Montreal, Canada; 2001:1–10.
20. Cervia F, Denti E, Galatolo R, Schettini F. Air Data Computation in Fly-By-Wire Flight Control Systems. *Journal of aircraft* 2006;43(2):450–5. doi:10.2514/1.16270.
21. Van Eykeren L, Chu Q. Fault Detection and Isolation for Inertial Reference Units. In: *AIAA Guidance,*

Navigation and Control Conference. AIAA 2013-4697; Boston, MA; 2013:1–10.

22. Lu P, Van Eykeren L, van Kampen E, Chu Q, Yu B. Adaptive Hybrid Unscented Kalman Filter for Aircraft Sensor Fault Detection , Isolation and Reconstruction. In: *AIAA Guidance, Navigation, and Control Conference*. AIAA 2014-1145; National Harbor, Maryland; 2014:1–18.
23. Van Eykeren L, Chu Q, Mulder JA. Sensor Fault Detection and Isolation using Adaptive Extended Kalman Filter. In: *8th IFAC Symposium on Fault Detection, Supervision and Safety of Technical Processes*. 1969; Mexico: IFAC, Laxenburg, Austria; 2012:1155–60.
24. Lu P, Van Eykeren L, van Kampen E, Chu Q. Selective-Reinitialization Multiple-Model Adaptive Estimation for Fault Detection and Diagnosis. *Journal of Guidance, Control, and Dynamics (in press)* 2015;.
25. Gillijns S, De Moor B. Unbiased Minimum-variance Input and State Estimation for Linear Discrete-time Systems with Direct Feedthrough. *Automatica* 2007;43(5):934–7. doi:10.1016/j.automatica.2006.11.016.
26. Lu P, van Kampen E. Aircraft Inertial Measurement Unit Fault Identification with Application to Real Flight Data. In: *AIAA Guidance, Navigation and Control Conference*. AIAA 2015-0859; Kissimmee, Florida; 2015:1–17.
27. Julier S, Uhlmann J. A New Extension of the Kalman Filter to Nonlinear Systems. In: *in Proceedings of AeroSense: The 11th Int. Symp. on Aerospace/Defence Sensing, Simulation and Control*. International Society for Optics and Photonics, USA; 1997:182–93.
28. Van Der Merwe R, Wan EA. The Square-root Unscented Kalman Filter for State and Parameter-estimation. In: *IEEE International Conference on Acoustics, Speech, and Signal Processing*. IEEE, Piscataway, NJ; 2001:3461–4.
29. Mehra RK. Approaches to Adaptive Filtering. *IEEE Transactions on Automatic Control* 1972;17(5):693–8. doi:10.1109/TAC.1972.1100100.
30. Soken HE, Hajiyev C. Pico satellite attitude estimation via Robust Unscented Kalman Filter in the presence of measurement faults. *ISA transactions* 2010;49(3):249–56. doi:10.1016/j.isatra.2010.04.001.
31. Goupil P. Oscillatory Failure Case Detection in the A380 Electrical Flight Control System by Analytical Redundancy. *Control Engineering Practice* 2010;18(9):1110–9. doi:10.1016/j.conengprac.2009.04.003.
32. Mulder J, Chu Q, Sridhar J. Non-linear Aircraft Flight Path Reconstruction Review and New Advances. *Progress in Aerospace Sciences* 1999;35:673–726. doi:10.1016/S0376-0421(99)00005-6.
33. de Visser CC. Global Nonlinear Model Identification with Multivariate Splines. Ph.D. thesis; Delft

University of Technology; 2011.

34. Lu P, Van Eykeren L, van Kampen E, de Visser CC, Chu Q. Double-Model Adaptive Fault Detection and Diagnosis Applied to Real Flight Data. *Control Engineering Practice* 2015;36:39–57. doi:10.1016/j.conengprac.2014.12.007.